Electronic Research Archive

http://www.aimspress.com/journal/era

ERA, 33(8): 4603–4624.
DOI: 10.3934/era.2025207
Received: 27 March 2025
Revised: 28 June 2025
Accepted: 22 July 2025
Published: 07 August 2025

Research article

Numerical study of bell–shaped solitons solutions for a generalized modified CH–DP equation

XiuMin Lyu[1] **and Qian Ge**[2,*]

[1] School of Science, Shandong Jiaotong University, Jinan 250357, China
[2] School of Science, Shandong Jianzhu University, Jinan 250101, China

* **Correspondence:** Email: geqian@sdjzu.edu.cn.

Abstract: In this paper, we developed a numerical scheme based on barycentric rational interpolation to solve the generalized modified Camassa–Holm–Degasperis–Procesi (CH–DP) equation. Using the proposed approach, we applied a direct linearization technique to transform the nonlinear generalized modified CH–DP equation into an equivalent linear formulation. Approximate solutions were constructed using barycentric rational interpolation basis functions. The spatiotemporal domain was discretized via barycentric rational interpolation, and a corresponding differentiation matrix was derived. Furthermore, theoretical analysis of error distribution and convergence properties was presented. Analytical results and numerical experiments validate the scheme's computational efficiency and high accuracy in solving the generalized modified CH–DP equation.

Keywords: numerical study; error estimate; direct linearization; barycentric rational collocation method; generalized modified CH–DP equation

1. Introduction

Nonlinear partial differential equations (PDEs) exhibit extensive applications across disciplines, including hydrodynamics, plasma physics, nonlinear optics, chemistry, and biology, particularly in modeling nonlinear wave phenomena. However, obtaining exact or numerical solutions for such equations remains challenging in most cases. This persistent difficulty has motivated sustained research efforts to develop analytical and computational methods for nonlinear PDEs. So far, relatively mature methods have been proposed, including hybrid analytical–numerical frameworks such as the homotopy perturbation method and variational iteration method [1], spectral domain decomposition for the Fisher equation [2], homotopy perturbation solutions for the Huxley equation [3], cubic B–spline quasi-interpolation schemes for Burgers' equation [4], finite difference methods for the Burgers–Huxley [5], and generalized Burgers–Fisher equations [6]. Spectral collocation methods have been successfully applied to nonlinear time–fractional Burgers' [7], time-fractional Schrödinger [8], and ψ–Hilfer fractional Black–Scholes equations [9]. Additionally, Chen et al. [10] proposed an alternating direction implicit compact difference scheme for two–dimensional integro–differential equations.

The Camassa–Holm (CH) and Degasperis–Procesi (DP) equations constitute two fundamental nonlinear PDEs in applied mathematics and theoretical physics. They exhibit strong nonlinear characteristics in describing shallow water wave propagation, integrable turbulence, and biophysical processes, particularly in simulating non–smooth wave phenomena that transcend the limitations of traditional KdV equations. Originating from Camassa and Holm's seminal work on shallow water wave dynamics, the CH equation incorporates dissipative and dispersive effects in wave evolution. Degasperis and Procesi subsequently extended this framework through the DP equation, introducing higher–order nonlinearities to model complex wave propagation. Moreover, researchers have generalized these frameworks into combined CH–DP type equations. These equations exhibit rich solution structures, including smooth solitons, singular traveling waves (peakons, cuspons, stumpons), and composite wave patterns, that challenge classical PDE analysis.

Analytical advances have significantly elucidated the solution spaces of these equations. Lenells [11] classified all weak traveling wave solutions of the CH equation, demonstrating the coexistence of smooth solitons with singular wave types. Parker and Matsuno [12] established peakons as limiting cases of CH solitons through asymptotic analysis, while Zhang and Zhang [13] revealed cuspon emergence under nonhomogeneous boundary conditions. The DP equation presents additional complexities through multi–peakon solutions [14], inverse scattering formulations [15], and multi–soliton structures [16]. Alquran et al. [17] derived novel bell–shaped and periodic soliton solutions using Kudryashov expansion and sech–csch function schemes. Abdel-Kader and Abdel-Latif [18] extended solution families via Lie symmetry analysis for coupled CH–DP systems. Lafortune and Pelinovsky [19] further demonstrated spectral instability of peakons in the b–family of CH equations. Sun et al. [20] investigated a four–parameter generalized CH–DP equation whose traveling wave system exhibits rich dynamical behaviors, yielding 30 distinct types of exact explicit bounded traveling wave solutions. Zhu et al. [21] established existence and uniqueness of global conservative weak solutions in $H^1(\mathbb{R})$ for cubic CH–type equations with nonlocal nonlinearity. Grunert [22] proved the uniqueness of dissipative solutions for the CH equation, establishing rigorous correspondence between energy dissipation and weak solution regularity. Numerical investigations have supplemented analytical progress through innovative discretization strategies. Liu and Ouyang [23] employed bifurcation analysis and numerical simulation to demonstrate the coexistence of bell–shaped solitary wave and peakons at identical wave speed. Behera and Mehra [24] developed wavelet–optimized finite difference schemes with adaptive resolution for CH equation singularities. Kaur et al. [25] proposed a coupled algorithm using fourth-order uniform algebraic tension B-splines and mixed block methods that convert PDEs to ordinary differential equations (ODEs) via differential quadrature, reducing grid points while maintaining high accuracy, significantly improving the computational efficiency of CH and DP equations. Qi et al. [26] proposed an invariant-preserving fourth–order finite difference scheme for the DP equation, achieving optimal error estimates for smooth solutions through matrix bounds and energy analysis. These analytical and numerical studies collectively address the challenges posed by the equations' nonlinearity and the multiplicity of solutions.

In recent years, the barycentric interpolation method has gained prominence due to its computational efficiency, numerical stability, and implementation simplicity. Some interpolated functions have been rewritten as the barycentric format with different weight functions [27, 28]. Moreover, the weighted stabilities of distinct barycentric–type interpolants at some special nodes have been analyzed in some literature [29, 30]. Crucially, when appropriate nodes such as Chebyshev nodes are selected, the method produces highly accurate results. Consequently, it has been widely adopted for diverse numerical challenges, such as Volterra integro–differential equations [31], nonlinear high–dimensional Fredholm integral equations [32], heat conduction [33], biharmonic [34], reaction–diffusion [35], and convection–diffusion equations [36]. Furthermore, Li and Wang [37, 38] successfully applied the barycentric interpolation method to practical engineering problems, including dynamic diffusion, vibration, and beam structural mechanics, as documented in their monographs.

Despite these advancements, applications of the linear barycentric rational collocation method to nonlinear wave equations, particularly the CH, DP, and CH–DP equations, remain notably limited. In this paper, we consider a general modified CH–DP equation [39, 40] given by

$$u_t - u_{xxt} + (\beta + 1)u^2 u_x = \beta u_x u_{xx} + u u_{xxx}, \tag{1.1}$$

where β is a positive integer and $u(x, t)$ denotes the fluid velocity's horizontal component. This equation inherits the peakon solution characteristics of the CH equation and the shock wave forming ability of the DP equation, providing a richer mathematical model for studying wave interactions and energy transfer mechanisms. Notably, for $\beta = 2$ and $\beta = 3$, Eq (1.1) reduces to the generalized modified CH and DP equations, respectively:

$$u_t - u_{xxt} + 3u^2 u_x = 2u_x u_{xx} + u u_{xxx}, \tag{1.2}$$

and

$$u_t - u_{xxt} + 4u^2 u_x = 3u_x u_{xx} + u u_{xxx}. \tag{1.3}$$

Wazwaz [39] pioneered the study of these modified forms, transforming the nonlinear convection term to $u^2 u_x$, which changes the characteristics of these peakon solutions, producing bell shaped solitary waves. Building on this foundation, we seek to explore the application of barycentric rational interpolation collocation to numerically solve these nonlinear wave equations.

The remainder of this paper is organized as follows: In Section 2, we develop a direct linearization technique for the generalized modified CH–DP equation and derive associated differentiation matrices. In Section 3, we establish error estimates for the linear barycentric rational collocation method applied to the generalized modified CH–DP equation. In Section 4, we present numerical examples validating the theoretical analysis. Finally, in Section 5, we summarize key findings and discuss their significance.

2. Numerical schemes

In this section, we utilize the barycentric interpolation method to aid in the resolution of the differentiation matrix formulation for the general modified CH–DP equation.

2.1. Direct linearization method for the generalized modified CH–DP equation

In the following, a direct linearization method is used to transform the nonlinear terms $u^2 u_x$ and $u_x u_{xx}$ into linear terms. Starting from an initial value $u^{(0)}$, we substitute it into the general modified

CH–DP equation and obtain:

$$u_t - u_{xxt} + (\beta + 1)(u^{(0)})^2 u_x - \beta(u^{(0)})_x u_{xx} - u^{(0)} u_{xxx} = 0. \tag{2.1}$$

Solving Eq (2.1) yields an updated value $u^{(1)}$. Similarly, replacing $u^{(0)}$ with $u^{(s-1)}$ at the s–th iteration ($s \in N^+$ represents the number of iterations), we establish a direct linear iteration scheme for the Eq (2.1):

$$u_t^{(s)} - u_{xxt}^{(s)} + (\beta + 1)(u^{(s-1)})^2 u_x^{(s)} - \beta(u^{(s-1)})_x u_{xx}^{(s)} - u^{(s-1)} u_{xxx}^{(s)} = 0. \tag{2.2}$$

In this context, $u^{(s-1)}$ denotes the value of u after $s-1$ iterations, while $u_t^{(s)}$ and $u_x^{(s)}$ represent the partial derivatives of u with respect to t and x after s iterations, respectively. Similarly, $(u^{(s-1)})_x$ represents the partial derivatives of u with respect to x after $s-1$ iterations, $u_{xx}^{(s)}$ and $u_{xxx}^{(s)}$ represent the second–order and third–order partial derivatives of u with respect to x after s iterations, respectively, and $u_{xxt}^{(s)}$ represents the third–order mixed partial derivatives of u with respect to x and t after s iterations.

2.2. Differentiation matrices for the generalized modified CH–DP equation

To approximate the general modified CH–DP equation, we adopt the barycentric interpolation collocation method. Both the time derivative and the spatial derivative terms are approximated.

Within the spatiotemporal domains $\Omega = [a, b] \times [0, T]$, we insert equidistant points (x_i, t_j), where $x_i = a + i\frac{b-a}{m}$ for $i = 1, 2, \cdots, m$ and $t_j = j\frac{T}{n}$ for $j = 1, 2, \cdots, n$, as well as the second kind of Chebyshev points (x_i, t_j), where $x_i = -\cos(\frac{i\pi}{m})$ for $i = 1, 2, \cdots, m$, and $t_j = -\cos(\frac{j\pi}{n})$ for $j = 1, 2, \cdots, n$. It is noteworthy that the Chebyshev nodes within the interval $[-1, 1]$ can be transformed to any interval $[a, b]$ via the linear transformation $\tilde{x} = \frac{b-a}{2}x + \frac{b+a}{2}$. In this case, the spatiotemporal domain Ω is divided into a uniform mesh with steps $h_x = \frac{b-a}{m}$ and $h_t = \frac{T}{n}$, and a non–uniform mesh with steps $h_i = x_i - x_{i-1}$ and $\tau_j = t_j - t_{j-1}$. The approximation $u_{mn}(x, t)$ to $u(x, t)$ is constructed as

$$u_{mn}(x, t) = \sum_{i=1}^{m} \sum_{j=1}^{n} \xi_i(x) \mu_j(t) u_{ij}, \tag{2.3}$$

where $u_{ij} = u(x_i, t_j)$, with interpolation basis functions

$$\xi_i(x) = \frac{\omega_i}{x - x_i} / \sum_{k=1}^{m} \frac{\omega_k}{x - x_k}, (i = 1, 2, \cdots, m), \quad \mu_j(t) = \frac{\omega_j}{t - t_j} / \sum_{k=1}^{n} \frac{\omega_k}{t - t_k}, (j = 1, 2, \cdots, n).$$

The barycentric interpolation weights ω_i and ω_j are computed as

$$\omega_i = \sum_{k_* \in J_i} (-1)^{k_*} \prod_{i_* = k_*, i_* \neq i}^{k_* + d_1} \frac{1}{x_i - x_{i_*}}, \quad \omega_j = \sum_{k_* \in J_j} (-1)^{k_*} \prod_{j_* = k_*, j_* \neq j}^{k_* + d_2} \frac{1}{t_j - t_{j_*}},$$

where $I_i = \{0, 1, 2, \cdots, m - d_1\}$, $J_i = \{k_* \in I_i : i - d_1 \leq k_* \leq i\}$, $I_j = \{0, 1, 2, \cdots, n - d_2\}$, and $J_j = \{k_* \in I_j : j - d_2 \leq k_* \leq j\}$. According to (2.3), the $(p + q)$–th partial derivative of the function $u_{mn}(x, t)$ is

$$\frac{\partial^{p+q} u_{mn}}{\partial x^p \partial t^q} = \sum_{i=1}^{m} \sum_{j=1}^{n} \xi_i^{(p)}(x) \mu_j^{(q)}(t) u_{ij}, (p, q = 0, 1, 2, \cdots). \tag{2.4}$$

Evaluating at nodes (x_g, t_h) yields:

$$u_{mn}^{(p,q)}(x_g, t_h) := \frac{\partial^{p+q} u_{mn}(x_g, t_h)}{\partial x^p \partial t^q} = \sum_{i=1}^{m} \sum_{j=1}^{n} \xi_i^{(p)}(x_g)\mu_j^{(q)}(t_h)u_{ij}, \tag{2.5}$$

for $g = 1, 2, \cdots, m, h = 1, 2, \cdots, n$, where $\xi_i^{(p)}$ and $\mu_j^{(q)}$ represent the p–th and q–th derivatives of interpolation basis function, respectively. The elements of the first–order and higher–order barycentric interpolation differentiation matrices are presented as follows [38]:

$$\xi_i'(x_k) = \begin{cases} \frac{\omega_i/\omega_k}{x_k - x_i}, \ k \neq i \\ -\sum\limits_{i=1, i\neq k}^{m} \xi_i'(x_k), \ k = i \end{cases}, \qquad \mu_j'(t_k) = \begin{cases} \frac{\omega_j/\omega_k}{t_k - t_j}, \ k \neq j \\ -\sum\limits_{j=1, j\neq k}^{n} \mu_j'(t_k), \ k = j \end{cases},$$

and

$$\xi_i^{(p)}(x_k) = \begin{cases} p(\xi_k^{(p-1)}(x_k)\xi_i'(x_k) - \frac{\xi_i^{(p-1)}(x_k)}{x_k - x_i}), \ k \neq i, \ p \geq 2 \\ -\sum\limits_{i=1, i\neq k}^{m} \xi_i^{(p)}(x_k), \ k = i, \ p \geq 2 \end{cases},$$

$$\mu_j^{(q)}(t_k) = \begin{cases} q(\mu_k^{(q-1)}(t_k)\mu_i'(t_k) - \frac{\mu_j^{(q-1)}(t_k)}{t_k - t_j}), \ k \neq j, \ q \geq 2 \\ -\sum\limits_{j=1, j\neq k}^{n} \mu_j^{(q)}(t_k), \ k = j, \ q \geq 2 \end{cases}.$$

Let $Dx_{ij}^{(m)} = \xi_j^{(m)}(x_i)$ and $Dt_{ij}^{(m)} = \mu_j^{(m)}(t_i)$ denote the m–th order derivative values of the j–th interpolation basis function at the i–th interpolation node in spatial and temporal directions, respectively. Thus, the algebraic summation (2.5) can be rewritten as

$$\mathbf{u}^{(p,q)} = (\mathbf{D}x^{(p)} \otimes \mathbf{D}t^{(q)})\mathbf{u} := \mathbf{D}^{(p,q)}\mathbf{u}, \tag{2.6}$$

where $\mathbf{D}x^{(0)} = \mathbf{I}_m$, $\mathbf{D}t^{(0)} = \mathbf{I}_n$, and $\otimes$ denotes the Kronecher product. Substituting (2.3) into (2.2), the differentiation matrices for the general modified CH–DP equation can be expressed as

$$[\mathbf{D}^{(0,1)} - \mathbf{D}^{(2,1)} + (\beta + 1)diag(\mathbf{u}^{(s-1)})^2\mathbf{D}^{(1,0)} - \beta diag(\mathbf{u}^{(s-1)}\mathbf{D}^{(1,0)})\mathbf{D}^{(2,0)} - diag(\mathbf{u}^{(s-1)})\mathbf{D}^{(3,0)}]\mathbf{u}^{(s)} = \mathbf{0}, \tag{2.7}$$

where $s = 1, 2, \cdots$. For simplicity, the matrix–vector multiplication in (2.7) can be represented as

$$\mathbf{LU} = \mathbf{0}, \tag{2.8}$$

with

$$\mathbf{L} = \mathbf{D}^{(0,1)} - \mathbf{D}^{(2,1)} + (\beta + 1)diag(\mathbf{u}^{(s-1)})^2\mathbf{D}^{(1,0)} - \beta diag(\mathbf{u}^{(s-1)}\mathbf{D}^{(1,0)})\mathbf{D}^{(2,0)} - diag(\mathbf{u}^{(s-1)})\mathbf{D}^{(3,0)},$$

and

$$\mathbf{U} = (u_{11}, \cdots, u_{1n}, u_{21}, \cdots, u_{2n}, \cdots, u_{m1}, \cdots, u_{mn})^T.$$

In general, the replacement method and addition method are often used to deal with initial–boundary conditions, as outlined in [38]. The discrete initial condition is as follows:

$$u(x_i, 0) = u_{i1} = u_0(x_i), \ i = 1, 2, \cdots, m, \tag{2.9}$$

with matrix representation:

$$\begin{bmatrix} u(x_1,0) \\ u(x_2,0) \\ \vdots \\ u(x_m,0) \end{bmatrix} = \begin{bmatrix} u_{11} \\ u_{21} \\ \vdots \\ u_{m1} \end{bmatrix} = (\mathbf{I}_m \otimes \mathbf{e}_n^1)\mathbf{U} = \begin{bmatrix} u_0(x_1) \\ u_0(x_2) \\ \vdots \\ u_0(x_m) \end{bmatrix}, \tag{2.10}$$

where $\mathbf{e}_n^1$ is the first row of an $n-$order identity matrix.

The boundary conditions are discretized as

$$u(a,t_j) = u_{1j} = g_1(t), \quad u(b,t_j) = u_{mj} = g_2(t), \quad j = 1,2,\cdots, n, \tag{2.11}$$

with corresponding matrix forms:

$$\begin{bmatrix} u(a,t_1) \\ u(a,t_2) \\ \vdots \\ u(a,t_n) \end{bmatrix} = \begin{bmatrix} u_{11} \\ u_{12} \\ \vdots \\ u_{1n} \end{bmatrix} = (\mathbf{e}_m^1 \otimes \mathbf{I}_n)\mathbf{U} = \mathbf{g}_1 = \begin{bmatrix} g_1(t_1) \\ g_1(t_2) \\ \vdots \\ g_1(t_n) \end{bmatrix}, \tag{2.12}$$

$$\begin{bmatrix} u(b,t_1) \\ u(b,t_2) \\ \vdots \\ u(b,t_n) \end{bmatrix} = \begin{bmatrix} u_{m1} \\ u_{m2} \\ \vdots \\ u_{mn} \end{bmatrix} = (\mathbf{e}_m^m \otimes \mathbf{I}_n)\mathbf{U} = \mathbf{g}_2 = \begin{bmatrix} g_2(t_1) \\ g_2(t_2) \\ \vdots \\ g_2(t_n) \end{bmatrix}. \tag{2.13}$$

In this context, $\mathbf{e}_m^1$ and $\mathbf{e}_m^m$ are the first row and the m-th row of an $m-$order identity matrix, respectively. In this study, we employ the additional method to address the initial and boundary conditions.

3. Error estimates

In this section, we establish error estimates and convergence properties for the barycentric rational collocation method applied to the generalized modified CH–DP equation, comparing exact solutions with numerical approximations.

We define the spatial error function as

$$e(x) := u(x) - u_m(x) = (x - x_i)\cdots(x - x_{i+d_1})u[x_i, x_{i+1}, \cdots, x_{i+d_1}, x], \tag{3.1}$$

where $u_m(x) = \sum\limits_{i=1}^{m} \xi_i(x)u_i$, with $u_i = u(x_i)$, and $\xi_i(x)$, defined in (2.3).

Lemma. Assume $u(x) \in C^{d+2}[a,b]$, let $h := \max\limits_{0\le i\le m-1}(x_{i+1} - x_i)$, and C be a positive constant. If $e(x)$ is as defined in (3.1), then

$$|e^{(k)}(x)| \le Ch^{d-k+1}, k = 0, 1, \cdots . \tag{3.2}$$

The proof of the lemma will not be elaborated here, as the detailed derivation process can be found in reference [41]. For the bivariate case, let $u(x,t)$ be the exact solution of Eq (1.1) and its approximation $u_{mn}(x,t)$ as defined in (2.3). The error function admits the representation:

$$\begin{aligned} e(x,t) :=& u(x,t) - u_{mn}(x,t) \\ =& (x - x_i)\cdots(x - x_{i+d_1})u[x_i, x_{i+1}, \cdots, x_{i+d_1}, x] + (t - t_j)\cdots(t - t_{j+d_2})u[t_j, t_{j+1}, \cdots, t_{j+d_2}, t]. \end{aligned} \tag{3.3}$$

Theorem 1. For $e(x,t)$ as defined in (3.3), with d_1, d_2 as defined in the symbols I_i, I_j, and $u(x,t) \in C^{(d+2)}(\Omega)$, where $\Omega = [a,b] \times [0,T]$, $d = \max\{d_1, d_2\}$, and C^* is a positive constant, we have

$$|e(x,t)^{(p,q)}| \leq C^*(h_x^{d_1-p+1} + h_t^{d_2-q+1}), p, q = 0, 1, \cdots , \tag{3.4}$$

where, $e(x,t)^{(p,q)}$ represents the p, q–order mixed partial derivatives of $e(x,t)$ with respect to x, t.

The detailed derivation process of Theorem 1 can be seen in reference [34]. Using the direct linearization method, the linearization operator corresponding to formula (2.1) is defined as

$$\ell := \frac{\partial}{\partial t} - \frac{\partial^3}{\partial x^2 \partial t} + (\beta+1)u_0^2 \frac{\partial}{\partial x} - \beta \frac{\partial u_0}{\partial x} \frac{\partial^2}{\partial x^2} - u_0 \frac{\partial^3}{\partial x^3}.$$

It can be shown that the operator ℓ is convergent and bounded. Let $u(x,t)$ be the solution of Eq (1.1) and $u(x_i, t_j)$ be the numerical solution obtained by the barycentric interpolation collocation method. Then,

$$\ell u(x_i, t_j) = 0, \tag{3.5}$$

and

$$\lim_{i,j\to\infty} \ell u(x_i, t_j) = 0.$$

Based on these results, we obtain the following Theorem 2.

Theorem 2. For $u(x_i, t_j) : \ell u(x_i, t_j) = 0$ and ℓ as defined above, we have

$$|u(x,t) - u(x_i, t_j)| \leq C(h_x^{d_1-2} + h_t^{d_2}), \tag{3.6}$$

where d_1, d_2 are as defined in the symbols I_i, I_j and C is a positive constant.

Proof: From Eq (3.5), we have

$$\begin{aligned}
&\ell u(x,t) - \ell u(x_i, t_j) \\
= \ & u_t(x,t) - u_{xxt}(x,t) + (\beta+1)u_0^2 u_x(x,t) - \beta \frac{\partial u_0}{\partial x} u_{xx}(x,t) - u_0 u_{xxx}(x,t) \\
& - [u_t(x_i,t_j) - u_{xxt}(x_i,t_j) + (\beta+1)u_0^2 u_x(x_i,t_j) - \beta \frac{\partial u_0}{\partial x} u_{xx}(x_i,t_j) - u_0 u_{xxx}(x_i,t_j)] \\
= \ & [u_t(x,t) - u_t(x_i,t_j)] + [-u_{xxt}(x,t) + u_{xxt}(x_i,t_j)] + (\beta+1)u_0^2[u_x(x,t) - u_x(x_i,t_j)] \\
& + \beta \frac{\partial u_0}{\partial x}[-u_{xx}(x,t) + u_{xx}(x_i,t_j)] + u_0[-u_{xxx}(x,t) + u_{xxx}(x_i,t_j)] \\
= \ & L_1 + L_2 + L_3 + L_4 + L_5,
\end{aligned} \tag{3.7}$$

where

$$\begin{aligned}
L_1 &= u_t(x,t) - u_t(x_i,t_j), \\
L_2 &= -u_{xxt}(x,t) + u_{xxt}(x_i,t_j), \\
L_3 &= (\beta+1)u_0^2[u_x(x,t) - u_x(x_i,t_j)], \\
L_4 &= \beta \frac{\partial u_0}{\partial x}[-u_{xx}(x,t) + u_{xx}(x_i,t_j)], \\
L_5 &= u_0[-u_{xxx}(x,t) + u_{xxx}(x_i,t_j)].
\end{aligned}$$

For L_1, we have

$$\begin{aligned} L_1 =&\ u_t(x,t) - u_t(x_i,t_j) \\ =&\ [u_t(x,t) - u_t(x_i,t)] + [u_t(x_i,t) - u_t(x_i,t_j)] \\ =&\ (x-x_i)\cdots(x-x_{i+d_1})u_t[x_i,x_{i+1},\cdots,x_{i+d_1},x,t] + (t-t_j)\cdots(t-t_{j+d_2})u_t[x_i,t_j,t_{j+1},\cdots,t_{j+d_2},t] \\ =&\ e_t(x_i,t) + e_t(x_i,t_j). \end{aligned} \tag{3.8}$$

Furthermore, based on the Theorem 1, we have

$$|L_1| \le |e_t(x_i,t)| + |e_t(x_i,t_j)| \le C_{11}^*(h_x^{d_1+1} + h_t^{d_2}) + C_{12}^*(h_x^{d_1+1} + h_t^{d_2}) = C_1(h_x^{d_1+1} + h_t^{d_2}), \tag{3.9}$$

where $C_1 = C_{11}^* + C_{12}^*$, C_{11}^* and C_{12}^* are positive constants.

Similarly, we have

$$|L_2| \le |e_{xxt}(x_i,t)| + |e_{xxt}(x_i,t_j)| \le C_2(h_x^{d_1-1} + h_t^{d_2}), \tag{3.10}$$

where C_1 and C_2 are positive constants. For L_3, we have

$$L_3 = (\beta+1)u_0^2[u_x(x,t) - u_x(x_i,t_j)] = (\beta+1)u_0^2[u_x(x,t) - u_x(x_i,t) + u_x(x_i,t) - u_x(x_i,t_j)], \tag{3.11}$$

then

$$|L_3| \le |(\beta+1)u_0^2|[|e_x(x_i,t)| + |e_x(x_i,t_j)|] \le C_3(h_x^{d_1} + h_t^{d_2+1}). \tag{3.12}$$

Similarly, we get

$$|L_4| \le |\beta\frac{\partial u_0}{\partial x}|[|e_{xx}(x_i,t)| + |e_{xx}(x_i,t_j)|] \le C_4(h_x^{d_1-1} + h_t^{d_2+1}), \tag{3.13}$$

$$|L_5| \le |u_0|[|e_{xxx}(x_i,t)| + |e_{xxx}(x_i,t_j)|] \le C_5(h_x^{d_1-2} + h_t^{d_2+1}), \tag{3.14}$$

where, C_3, C_4, and C_5 are positive constants. Combining Eqs (3.8)–(3.14), we have

$$|u(x,t) - u(x_i,t_j)| \le |L_1| + |L_2| + |L_3| + |L_4| + |L_5| \le C(h_x^{d_1-2} + h_t^{d_2}),$$

where $C := \max\{C_1, C_2, C_3, C_4, C_5\}$. Thus, the proof is completed.

4. Numerical experiments and discussion

In this study, the generalized modified CH–DP equation (1.1) is numerically solved only for bell–shaped soliton solutions [39]. Barycentric interpolation basis functions are constructed using Chebyshev nodes and compared with equidistant nodes to summarize the conditions of stability. The standard Chebyshev domain $[-1,1]$ is mapped to the physical spatial interval $[a,b]$ and temporal domain $[0,T]$ via coordinate transformation formulas $\tilde{x} = \frac{b-a}{2}x + \frac{b+a}{2}$ and $\tilde{t} = \frac{T}{2}t + \frac{T}{2}$. The maximum absolute error E_∞, relative error E_r, and convergence orders in space (h^*) and time (t^*) are defined as follows:

$$E_\infty = \|U^e - U^c\|_\infty = \max_k |U_k^e - U_k^c|, \quad E_r = \frac{\|U^e - U^c\|_\infty}{\|U^e\|_\infty},$$

$$h^* = \frac{\log\frac{E_i}{E_{i+1}}}{\log\frac{h_i}{h_{i+1}}}, \quad t^* = \frac{\log\frac{E_i}{E_{i+1}}}{\log\frac{\tau_i}{\tau_{i+1}}},$$

where U^e and U^c denote the exact and computed solutions of $u(x,t)$, respectively, E_i represents the error at the i–th mesh resolution, and h_i and τ_i represent the maximum spatial and temporal step sizes for the corresponding discretization.

The exact bell–shaped soliton solution for the generalized modified CH-DP equation (1.1) is given by [39]:

$$u(x,t) = -\frac{3(\beta+2)}{2(\beta+1)} sech^2[\frac{1}{2}(x - \frac{\beta+2}{2}t)].$$

Subsequently, we present some numerical experiments for specific β values to validate the efficacy and applicability of the barycentric interpolation collocation method.

Example 1. *Let $\beta = 2$, we consider the generalized modified CH equation* (1.2)

$$u_t - u_{xxt} + 3u^2 u_x - 2u_x u_{xx} - u u_{xxx} = 0,$$

defined on the domain $\Omega = [a,b] \times [0,T]$. The exact bell–shaped soliton solution is

$$u(x,t) = -2sech^2(\frac{x-2t}{2}), \tag{4.1}$$

with the initial condition

$$u(x,0) = -2sech^2(\frac{x}{2}).$$

For Example 1, the temporal evolution of bell-shaped soliton solutions for the generalized modified CH equation are presented in Figure 1. Within the computational domain $\Omega = [-5,5] \times [0,0.1]$, Figure 2 demonstrates excellent agreement between the numerical solutions computed on uniform and non–uniform grids against the exact solution in Eq (4.1).

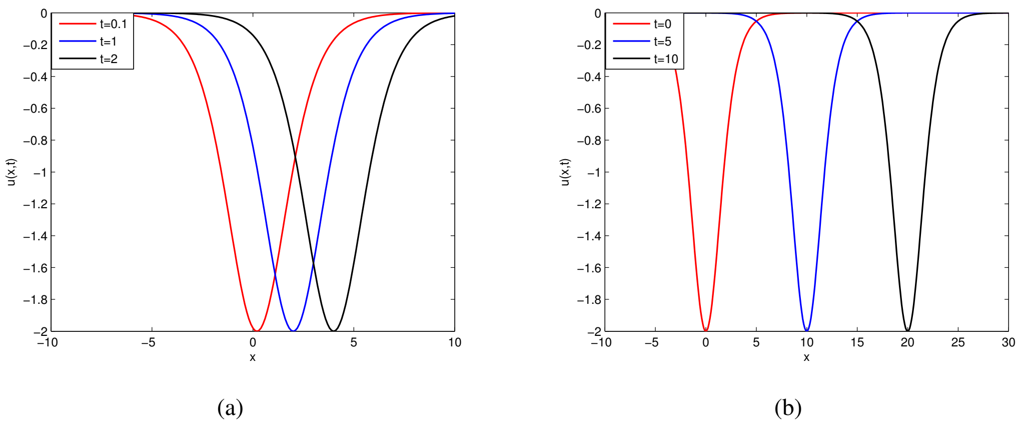

Figure 1. The temporal evolution of bell–shaped soliton solution for Example 1.

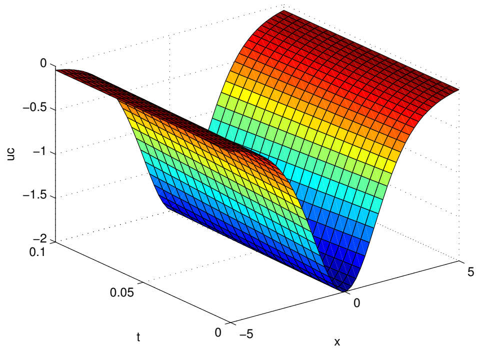

(a) Uniform mesh: 51×20 equidistant nodes

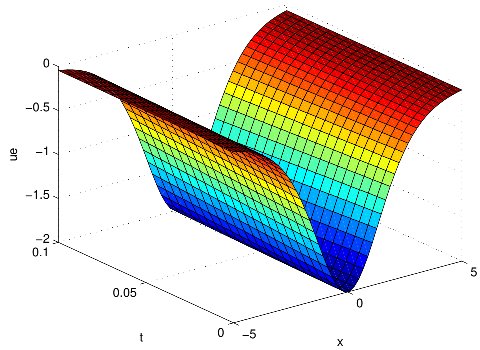

(b) Bell-shaped soliton solution

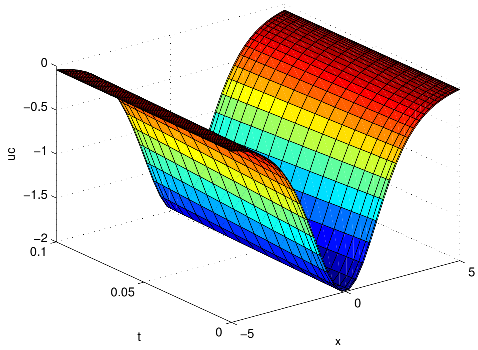

(c) Non-uniform mesh: 51×20 Chebyshev nodes

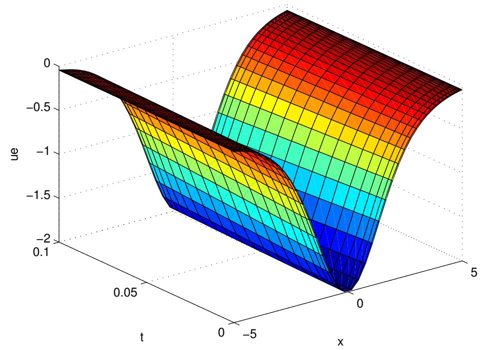

(d) Bell-shaped soliton solution

Figure 2. Numerical solution and bell-shaped soliton solution of the generalized modified CH equation for Example 1.

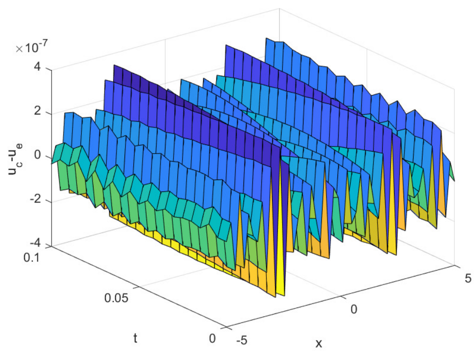

(a) Equidistant nodes

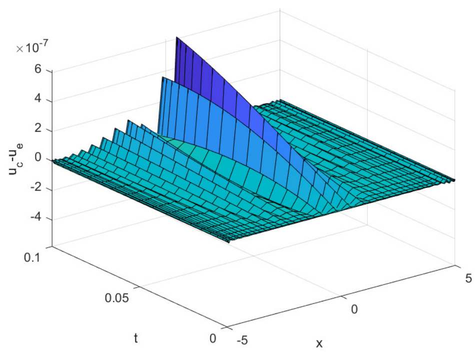

(b) Chebyshev nodes

Figure 3. Error distribution calculated by different types of nodes with $m \times n = 51 \times 20$, $d_1 = 4$, and $d_2 = 6$ for Example 1.

Figure 3 depicts the maximum absolute error distributions from the barycentric interpolation collocation method using equidistant and Chebyshev nodes. It is clear that the numerical solutions obtained through barycentric rational collocation method approximate the bell–shaped soliton solution with high accuracy. Notably, the barycentric rational interpolation with Chebyshev nodes maintains stable numerical precision, while equidistant interpolation exhibits oscillatory behavior, as shown in Figure 3.

Table 1. Maximum absolute error and relative error calculated by different types of interpolation method with $d_1 = 5$, $d_2 = 6$, and $\Omega = [-5, 5] \times [0, 0.1]$ for Example 1.

Error	$m \times n$	Chebyshev	Equidistant	$m \times n$	Chebyshev	Equidistant
	18×10	$3.4602e-04$	$1.9104e-04$	30×10	$9.5774e-07$	$2.7444e-06$
	26×10	$4.5201e-06$	$6.4967e-06$	30×14	$8.3786e-07$	$2.7797e-06$
E_∞	34×10	$2.9695e-07$	$1.1436e-06$	30×18	$7.2669e-07$	$2.8189e-06$
	42×10	$9.2886e-08$	$2.6480e-07$	30×22	$6.2321e-07$	$2.8557e-06$
	18×10	$1.7301e-04$	$9.5520e-05$	30×10	$4.7887e-07$	$1.3722e-06$
	26×10	$2.2600e-06$	$3.2484e-06$	30×14	$4.1893e-07$	$1.3899e-06$
E_r	34×10	$1.4848e-07$	$5.7180e-07$	30×18	$3.6334e-07$	$1.4094e-06$
	42×10	$4.6443e-08$	$1.3240e-07$	30×22	$3.1161e-07$	$1.4278e-06$

Table 2. Maximum absolute errors calculated by the barycentric rational collocation method for different t with $d_1 = 5$, $d_2 = 4$, $m \times n = 35 \times 20$ for Example 1.

Node type	$t = 0.05$	$t = 0.1$	$t = 0.5$	$t = 1$	$t = 2$
Chebyshev	$7.2327e-07$	$1.3847e-06$	$5.5260e-06$	$1.3328e-05$	$3.1023e-03$
Equidistant	$4.7817e-07$	$5.4986e-07$	$2.0118e-05$	$7.7540e-04$	–

Table 3. Maximum absolute errors calculated by the barycentric Lagrange interpolation method for different t with $m \times n = 35 \times 20$ for Example 1.

Node type	$t = 0.05$	$t = 0.1$	$t = 0.5$	$t = 1$	$t = 2$
Chebyshev	$2.2835e-06$	$2.3045e-05$	$2.1479e-04$	$7.0759e-03$	$1.7756e-02$
Equidistant	–	–	–	–	–

The general modified CH equation is solved using the barycentric rational interpolation method with Chebyshev nodes and equidistant nodes, respectively. Generally, numerical results obtained through Chebyshev node interpolation display a distinct advantage compared to those from equidistant node interpolation. As shown in Table 1, increasing the number of nodes in the x–direction enhances numerical accuracy while maintaining stability. In the t–direction, high computational accuracy is achieved once the node count exceeds a certain threshold.

Data in Table 2 indicate that the accuracy of Chebyshev nodes interpolation remains relatively stable as time t increases, particularly under long-term conditions, in comparison to equidistant nodes interpolation. For example, at $t = 2$, the accuracy of the Chebyshev nodes interpolation reaches the magnitude of 10^{-3}, whereas the equidistant nodes interpolation exhibits poor precision and cannot even achieve the magnitude 10^{-1}.

In addition, under the same parameter conditions, the barycentric Lagrange interpolation method is applied to Example 1. With equidistant nodes $m \times n = 20 \times 10$, the maximum absolute error is 2.7073×10^{-2}. However, when the number of equidistant nodes increases to $m \times n = 35 \times 20$, numerical calculation results are distorted. These results are presented in Table 3.

From the comparative analysis of the numerical results in Tables 2 and 3, it can be seen that that when applying the barycentric Lagrange interpolation method, if the nodes are dense or close, the weights of the basis functions may approach zero or diverge, leading to ill conditioned coefficient matrices and unreliable interpolation results. Compared with the barycentric Lagrange interpolation method, the barycentric rational interpolation method solves the problems of Runge phenomenon and numerical instability, and has better approximation ability and higher numerical stability.

Table 4. Maximum absolute errors and convergence orders calculated by Chebyshev interpolation nodes with $d_2 = 6$, $t = 0.1$ for Example 1.

$m \times n$	$d_1 = 5$	h^*	$d_1 = 4$	h^*	$d_1 = 3$	h^*	$d_1 = 2$	h^*
21×20	$6.3283e-05$		$8.2930e-05$		$7.3608e-05$		$2.5556e-04$	
27×20	$6.5546e-06$	9.02	$1.5957e-05$	6.56	$2.3891e-05$	4.48	$1.3213e-04$	2.63
33×20	$1.9631e-06$	6.01	$5.7483e-06$	5.09	$8.1517e-06$	5.36	$9.8317e-05$	1.47
39×20	$7.2448e-07$	5.97	$2.2407e-06$	5.64	$2.9626e-06$	6.06	$6.9305e-05$	2.09
45×20	$3.2094e-07$	5.69	$1.2015e-06$	4.35	$2.7993e-06$	–	$5.0374e-05$	2.23
51×20	$1.7470e-07$	4.86	$6.1141e-07$	5.40	$1.7297e-06$	3.85	$2.9607e-05$	4.25

Table 5. Maximum absolute errors and convergence orders calculated by equidistant interpolation nodes with $d_2 = 6$, $t = 0.1$ for Example 1.

$m \times n$	$d_1 = 5$	h^*	$d_1 = 4$	h^*	$d_1 = 3$	h^*	$d_1 = 2$	h^*
21×20	$1.1954e-05$		$5.5658e-05$		$1.0240e-04$		$2.7866e-04$	
27×20	$5.1873e-06$	3.32	$2.2850e-05$	3.54	$6.5115e-05$	1.80	$1.4551e-04$	2.59
33×20	$9.4535e-07$	8.48	$5.3247e-06$	7.26	$2.2270e-05$	5.35	$1.0417e-04$	1.67
39×20	$2.2660e-07$	8.55	$1.3657e-06$	8.15	$8.0633e-06$	6.08	$7.7655e-05$	1.76
45×20	$1.0624e-07$	5.29	$5.9125e-07$	5.85	$4.1726e-06$	4.60	$5.0052e-05$	3.07
51×20	$4.7631e-08$	6.41	$3.4880e-07$	4.22	$3.0822e-06$	2.42	$3.5363e-05$	2.78

Table 6. Maximum absolute errors and convergence orders calculated by Chebyshev interpolation nodes with $d_1 = 5$, $t = 0.1$ for Example 1.

$m \times n$	$d_2 = 4$	t^*	$d_2 = 3$	t^*	$d_2 = 2$	t^*	$d_2 = 1$	t^*
35×10	$1.4039e-06$		$1.3992e-06$		$3.5595e-05$		$4.9310e-04$	
35×14	$1.3961e-06$	–	$1.3951e-06$	–	$1.2603e-05$	3.09	$3.3613e-04$	1.14
35×18	$1.3884e-06$	–	$1.3881e-06$	–	$5.7975e-06$	3.09	$2.5431e-04$	1.11
35×22	$1.3812e-06$	–	$1.3807e-06$	–	$3.1202e-06$	3.09	$2.0433e-04$	1.09
35×26	$1.3743e-06$	–	$1.3742e-06$	–	$1.8644e-06$	3.08	$1.7068e-04$	1.08

Table 7. Maximum absolute errors and convergence orders calculated by equidistant interpolation nodes with $d_1 = 5$, $t = 0.1$ for Example 1.

$m \times n$	$d_2 = 4$	t^*	$d_2 = 3$	t^*	$d_2 = 2$	t^*	$d_2 = 1$	t^*
35×10	$5.4626e-07$		$5.4518e-07$		$6.7844e-05$		$1.2511e-03$	
35×14	$5.4822e-07$	–	$5.4775e-07$	–	$3.5586e-05$	1.92	$9.5744e-04$	0.80
35×18	$5.4940e-07$	–	$5.4922e-07$	–	$2.1999e-05$	1.91	$7.8638e-04$	0.78
35×22	$5.5024e-07$	–	$5.5022e-07$	–	$1.4921e-05$	1.93	$6.7260e-04$	0.78
35×26	$5.5088e-07$	–	$5.5098e-07$	–	$1.0735e-05$	1.97	$5.9042e-04$	0.78

Tables 4 and 5 display the convergence rates of the spatial variable for Chebyshev node interpolations and equidistant node interpolations, respectively, with the time interpolation parameter set at $d_2 = 6$. Conversely, Tables 6 and 7 present the convergence rates of the temporal variable for both interpolation methods, with the spatial interpolation parameter fixed at $d_1 = 5$. An analysis of Tables 3 to 6 reveal that for both Chebyshev and equidistant nodes, the spatial convergence rate is $O(h_x^{d_1+1})$ with $d_2 = 6$ and d_1 ranging from 2 to 5, while the temporal convergence rate is $O(h_t^{d_2})$ with $d_1 = 5$ and d_2 ranging from 1 to 4, all of which are consistent with our theoretical analysis.

Example 2. *Let $\beta = 3$, and we consider the generalized modified DP equation* (1.3)

$$u_t - u_{xxt} + 4u^2 u_x - 3u_x u_{xx} - u u_{xxx} = 0,$$

defined on the domain $\Omega = [-5, 5] \times [0, 0.1]$. The exact bell–shaped soliton solution and initial condition are

$$u(x,t) = -\frac{15}{8} sech^2(\frac{2x - 5t}{4}) \text{ and } u(x,0) = -\frac{15}{8} sech^2(\frac{x}{2}).$$

Consistent with Example 1, Figure 4 displays the temporal evolution of the exact bell–shaped soliton solutions for the generalized modified DP equation. Figure 5 displays numerical solutions on 51×20 uniform and non–uniform meshes, demonstrating close agreement with the exact solution. Furthermore, error distributions are illustrated in Figure 6, revealing stable accuracies for Chebyshev nodes versus oscillatory errors for equidistant nodes.

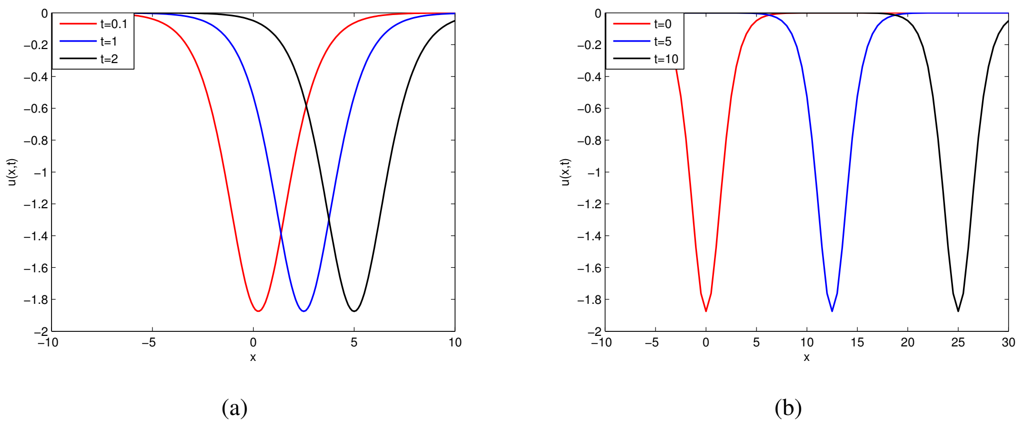

Figure 4. The temporal evolution of bell–shaped soliton solution for Example 2.

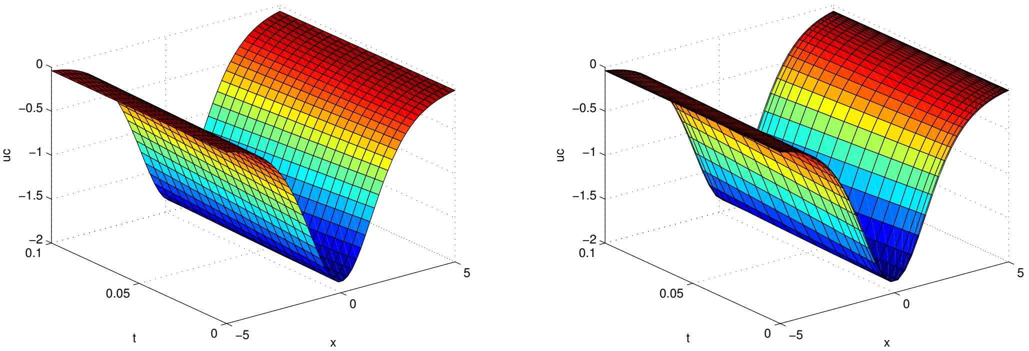

(a) Uniform mesh: 51×20 equidistant nodes (b) Non-uniform mesh: 51×20 Chebyshev nodes

Figure 5. Numerical solution of the generalized modified DP equation for Example 2.

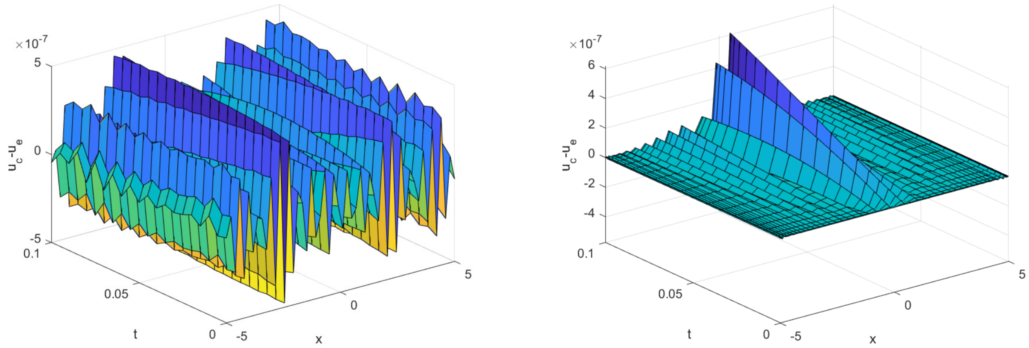

(a) Equidistant nodes (b) Chebyshev nodes

Figure 6. Error distribution calculated by different types of nodes with $m \times n = 51 \times 20$, $d_1 = 4$, and $d_2 = 6$ for Example 2.

Furthermore, the data in Table 8 confirm that Chebyshev interpolation exhibits superior stability and effectiveness over equidistant interpolation when solving the generalized modified DP equation via the barycentric interpolation collocation method. Analysis of Tables 9 to 12 show that with time interpolation parameter $d_2 = 6$, the spatial convergence rate achieves $O(h_x^{d_1+1})$ for $d_1 = 2, 3, 4, 5$. When $d_1 = 5$, the temporal convergence rate attains $O(h_t^{d_2})$ for $d_2 = 1, 2, 3, 4$. These results are consistent with our theoretical analysis.

Table 8. Maximum absolute errors and relative errors calculated by different types of interpolation methods with $d_1 = 5$, $d_2 = 6$, $\Omega = [-5, 5] \times [0, 0.1]$ for Example 2.

Error	$m \times n$	Chebyshev	Equidistant	$m \times n$	Chebyshev	Equidistant
	18×20	$3.3184e-04$	$2.4191e-04$	35×10	$1.2629e-06$	$9.6294e-07$
	27×20	$5.9818e-06$	$8.5059e-06$	35×14	$1.2548e-06$	$9.6634e-07$
E_∞	36×20	$1.1792e-07$	$8.0333e-07$	35×18	$1.2474e-06$	$9.6785e-07$
	45×20	$2.7009e-07$	$1.3389e-07$	35×22	$1.2408e-06$	$9.6838e-07$
	18×20	$1.7698e-04$	$1.2902e-04$	35×10	$6.7352e-07$	$5.1357e-07$
	27×20	$3.1916e-06$	$4.5365e-06$	35×14	$6.6923e-07$	$5.1538e-07$
E_r	36×20	$6.2889e-07$	$4.2845e-07$	35×18	$6.6528e-07$	$5.1619e-07$
	45×20	$1.4405e-07$	$7.1409e-08$	35×22	$6.6175e-07$	$5.1647e-07$

Table 9. Maximum absolute errors and convergence orders calculated by Chebyshev interpolation nodes with $d_2 = 6$, $t = 0.1$ for Example 2.

$m \times n$	$d_1 = 5$	h^*	$d_1 = 4$	h^*	$d_1 = 3$	h^*	$d_1 = 2$	h^*
21×20	$6.7370e-05$		$8.5459e-05$		$8.8317e-05$		$3.0205e-04$	
27×20	$5.9818e-06$	9.64	$1.4568e-05$	7.04	$2.5154e-05$	5.00	$1.2255e-04$	3.59
33×20	$1.7525e-06$	6.12	$5.4684e-06$	4.88	$8.1639e-06$	5.61	$9.5680e-05$	1.23
39×20	$6.5407e-07$	5.90	$1.9790e-06$	6.08	$2.1493e-06$	7.99	$6.4003e-05$	2.41
45×20	$2.7009e-07$	6.18	$9.9255e-07$	4.82	$2.6832e-06$	-1.55	$4.9146e-05$	1.85
51×20	$1.4793e-07$	4.81	$6.1372e-07$	3.84	$1.9701e-06$	2.47	$2.6894e-05$	4.82

Table 10. Maximum absolute errors and convergence orders calculated by equidistant interpolation nodes with $d_2 = 6$, $t = 0.1$ for Example 2.

$m \times n$	$d_1 = 5$	h^*	$d_1 = 4$	h^*	$d_1 = 3$	h^*	$d_1 = 2$	h^*
21×20	$1.9105e-05$		$9.2142e-05$		$1.3066e-04$		$2.7432e-04$	
27×20	$8.5059e-06$	3.22	$2.4156e-05$	3.95	$8.5728e-05$	1.68	$1.2193e-04$	3.23
33×20	$1.3376e-06$	8.12	$8.9971e-06$	6.65	$2.9738e-05$	5.28	$8.7081e-05$	1.68
39×20	$3.5729e-07$	9.22	$2.3011e-06$	8.16	$1.0163e-05$	6.43	$6.7221e-05$	1.55
45×20	$1.3150e-07$	6.98	$7.9949e-07$	7.39	$4.7138e-06$	5.37	$4.3448e-05$	3.05
51×20	$7.2048e-08$	4.81	$4.9280e-07$	3.87	$3.2881e-06$	2.88	$3.0374e-05$	2.86

Table 11. Maximum absolute errors and convergence orders calculated by Chebyshev interpolation nodes with $d_1 = 5$, $t = 0.1$ for Example 2.

$m \times n$	$d_2 = 4$	t^*	$d_2 = 3$	t^*	$d_2 = 2$	t^*	$d_2 = 1$	t^*
35×10	$1.2595e-06$		$1.2401e-06$		$8.1056e-05$		$1.1223e-03$	
35×14	$1.2543e-06$	–	$1.2506e-06$	–	$2.8641e-05$	3.09	$7.6483e-04$	1.14
35×18	$1.2472e-06$	–	$1.2460e-06$	–	$1.3159e-05$	3.09	$5.7854e-04$	1.11
35×22	$1.2405e-06$	–	$1.2401e-06$	–	$7.0900e-06$	3.08	$4.6475e-04$	1.09
35×26	$1.2342e-06$	–	$1.2345e-06$	–	$4.2414e-06$	3.08	$3.8819e-04$	1.08
35×30	$1.2290e-06$	–	$1.2289e-06$	–	$2.7328e-06$	3.07	$3.3320e-04$	1.07

Table 12. Maximum absolute errors and convergence orders calculated by equidistant interpolation nodes with $d_1 = 5$, $t = 0.1$ for Example 2.

$m \times n$	$d_2 = 4$	t^*	$d_2 = 3$	t^*	$d_2 = 2$	t^*	$d_2 = 1$	t^*
35×10	$9.6092e-07$		$9.6111e-07$		$1.5259e-04$		$2.8113e-03$	
35×14	$9.6381e-07$	–	$9.6278e-07$	–	$8.0000e-05$	1.92	$2.1514e-03$	0.80
35×18	$9.6530e-07$	–	$9.6421e-07$	–	$4.9461e-05$	1.91	$1.7671e-03$	0.78
35×22	$9.6595e-07$	–	$9.6489e-07$	–	$3.3562e-05$	1.93	$1.5117e-03$	0.78
35×26	$9.6609e-07$	–	$9.6506e-07$	–	$2.4158e-05$	1.97	$1.3272e-03$	0.78
35×30	$9.6589e-07$	–	$9.6485e-07$	–	$1.8105e-06$	2.02	$1.1864e-03$	0.78

Example 3. *Let $\beta = 4$, and we consider the generalized modified CH-DP equation* (1.1)

$$u_t - u_{xxt} + 5u^2 u_x - 4u_x u_{xx} - uu_{xxx} = 0,$$

defined on the domain $\Omega = [-5, 5] \times [0, 0.1]$. The exact bell–shaped soliton solution and initial condition are

$$u(x,t) = -\frac{15}{8} sech^2(\frac{2x-5t}{4}) \text{ and } u(x,0) = -\frac{9}{5} sech^2(\frac{x}{2}).$$

The nonlinear generalized modified CH–DP equation (1.1) is solved via the barycentric interpolation collocation method. Figures 7–9 present temporal evolution of bell–shaped soliton solutions, numerical solutions $u(x,t)$ on 51×20 uniform and non–uniform meshes, and maximum absolute error distributions for equidistant and Chebyshev nodes, respectively.

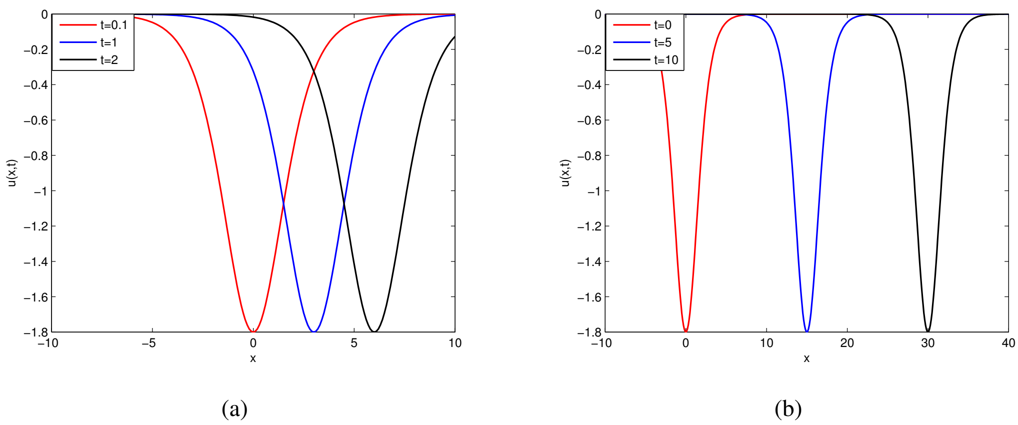

Figure 7. The temporal evolution of bell–shaped soliton solution for Example 3.

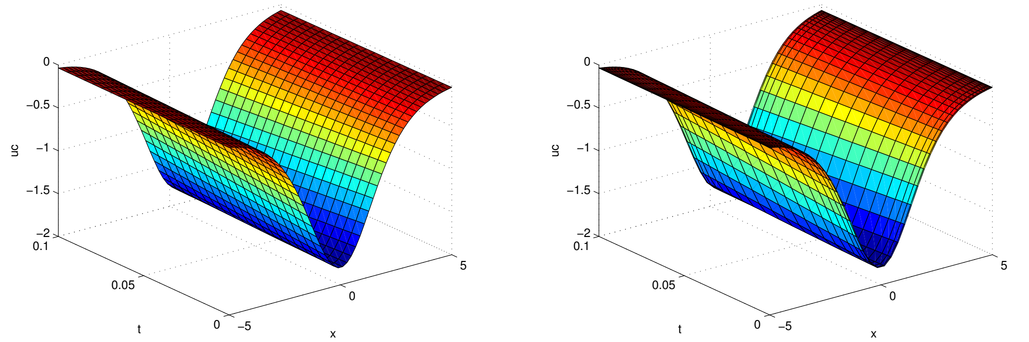

(a) Uniform mesh: 51×20 equidistant nodes (b) Non-uniform mesh: 51×20 Chebyshev nodes

Figure 8. Numerical solution of the generalized modified CH-DP equation for Example 3.

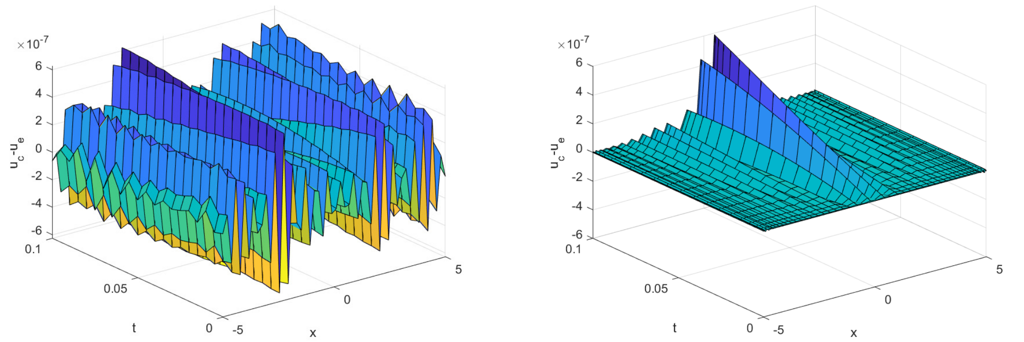

(a) Equidistant nodes (b) Chebyshev nodes

Figure 9. Error distribution calculated by different types of nodes with $m \times n = 51 \times 20$, $d_1 = 4$, and $d_2 = 6$ for Example 3.

Table 13. Maximum absolute errors and relative errors calculated by different types of interpolation methods with $d_1 = 5$, $d_2 = 6$, $\Omega = [-5, 5] \times [0, 0.1]$ for Example 3.

Error	$m \times n$	Chebyshev	Equidistant	$m \times n$	Chebyshev	Equidistant
	18×20	$3.4242e-04$	$4.2042e-04$	35×10	$1.1807e-06$	$1.5076e-06$
	27×20	$5.6503e-06$	$1.1512e-05$	35×14	$1.1719e-06$	$1.5155e-06$
E_∞	36×20	$1.3451e-07$	$8.5864e-07$	35×18	$1.1641e-06$	$1.5203e-06$
	45×20	$2.4028e-07$	$1.7210e-07$	35×22	$1.1575e-06$	$1.5233e-06$
	18×20	$1.9023e-04$	$2.3357e-04$	35×10	$6.5600e-07$	$8.3756e-07$
	27×20	$3.1391e-06$	$6.3956e-06$	35×14	$6.5104e-07$	$8.4197e-07$
E_r	36×20	$7.4730e-07$	$4.7702e-07$	35×18	$6.4672e-07$	$8.4461e-07$
	45×20	$1.3349e-07$	$9.5610e-08$	35×22	$6.4304e-07$	$8.4631e-07$

Table 14. Maximum absolute errors and convergence orders calculated by Chebyshev interpolation nodes with $d_2 = 6$, $t = 0.1$ for Example 3.

$m \times n$	$d_1 = 5$	h^*	$d_1 = 4$	h^*	$d_1 = 3$	h^*	$d_1 = 2$	h^*
21×20	$6.6963e-05$		$7.8614e-05$		$1.2037e-05$		$3.5639e-04$	
27×20	$5.6503e-06$	9.84	$1.4086e-05$	6.84	$2.6204e-05$	6.07	$1.1477e-04$	4.51
33×20	$1.6394e-06$	6.17	$5.4092e-06$	4.77	$9.2336e-06$	5.20	$9.5632e-05$	0.91
39×20	$6.1459e-07$	5.87	$1.8495e-06$	6.42	$1.7976e-06$	9.80	$6.6989e-05$	2.13

Table 15. Maximum absolute errors and convergence orders calculated by equidistant interpolation nodes with $d_2 = 6$, $t = 0.1$ for Example 3.

$m \times n$	$d_1 = 5$	h^*	$d_1 = 4$	h^*	$d_1 = 3$	h^*	$d_1 = 2$	h^*
21×20	$3.8411e-05$		$1.6375e-04$		$1.8569e-04$		$3.1000e-04$	
27×20	$1.1512e-05$	4.79	$4.4214e-05$	5.21	$1.0785e-04$	2.16	$1.2519e-04$	3.61
33×20	$2.5413e-06$	7.53	$1.3289e-05$	5.99	$4.2557e-05$	4.63	$8.0919e-05$	2.17
39×20	$5.5095e-07$	9.15	$3.4894e-06$	8.00	$1.4386e-05$	6.49	$6.1823e-05$	1.61

Table 16. Maximum absolute errors and convergence orders calculated by Chebyshev interpolation nodes with $d_1 = 5$, $t = 0.1$ for Example 3.

$m \times n$	$d_2 = 4$	t^*	$d_2 = 3$	t^*	$d_2 = 2$	t^*	$d_2 = 1$	t^*
35×10	$1.1711e-06$		$1.1146e-06$		$1.6253e-04$		$2.2534e-03$	
35×14	$1.1710e-06$	–	$1.1602e-06$	–	$5.7474e-05$	3.09	$1.5355e-03$	1.14
35×18	$1.6390e-06$	–	$1.1609e-06$	–	$2.6341e-05$	3.10	$1.1614e-03$	1.11
35×22	$1.1568e-06$	–	$1.1558e-06$	–	$1.4160e-05$	3.09	$9.3294e-04$	1.09
35×26	$1.1508e-06$	–	$1.1500e-06$	–	$8.4718e-06$	3.07	$7.7914e-04$	1.08

Table 17. Maximum absolute errors and convergence orders calculated by equidistant interpolation nodes with $d_1 = 5$, $t = 0.1$ for Example 3.

$m \times n$	$d_2 = 4$	t^*	$d_2 = 3$	t^*	$d_2 = 2$	t^*	$d_2 = 1$	t^*
35×10	$1.5061e-06$		$1.5084e-06$		$3.0514e-04$		$5.6105e-03$	
35×14	$1.5138e-06$	–	$1.5129e-06$	–	$1.5989e-04$	1.92	$4.2938e-03$	0.79
35×18	$1.5187e-06$	–	$1.5176e-06$	–	$9.8841e-05$	1.91	$3.5273e-03$	0.78
35×22	$1.5219e-06$	–	$1.5209e-06$	–	$6.7085e-05$	1.93	$3.0179e-03$	0.78
35×26	$1.5240e-06$	–	$1.5231e-06$	–	$4.8318e-05$	1.96	$2.6503e-03$	0.78

Numerical results for different Chebyshev and equidistant interpolation nodes are presented in Tables 13 to 17. The convergence results are also displayed in Tables 14 to 17. It is observed that for both Chebyshev and equidistant nodes, the spatial convergence rate is $O(h_x^{d_1+1})$ with $d_2 = 6$ and $d_1 = 2, 3, 4, 5$, while the temporal convergence rate is $O(h_t^{d_2})$ with $d_1 = 5$, $d_2 = 1, 2$. These findings align with theoretical analysis.

5. Concluding remarks

In this paper, we present a numerical algorithm based on barycentric rational interpolation for approximating bell-shaped soliton solutions of the general modified CH–DP equation. The barycentric interpolant and its differentiation matrix discretize unknown functions without mesh generation, significantly simplifying implementation. Error estimation and convergence analysis establish spatial convergence rates of $O(h_x^{d_1-1})$ and temporal rates of $O(h_t^{d_2})$ for equidistant interpolation. Numerical experiments demonstrate the scheme's efficacy and accuracy in solving the general modified CH–DP equation, with results consistent with theoretical analysis. Compared to existing methods, the proposed approach achieves higher accuracy with fewer nodes while reducing computational costs. We focus on bell-shaped soliton solutions, and in the future, we will investigate peakon solitary wave solutions and extend this to high-dimensional problems such as nonlinear parabolic evolution equations [42].

Use of AI tools declaration

The authors declare they have not used Artificial Intelligence (AI) tools in the creation of this article.

Acknowledgments

The work was supported by the Natural Science Foundation of Shandong Province (Grant No. ZR2022MA003).

The authors also gratefully acknowledges the helpful comments and suggestions of the reviewers, which have improved the presentation.

Conflicts of interest

All authors declare no conflict of interest.

References

1. M. A. Yousif, B. A. Mahmood, F. H. Easif, A new analytical study of modified Camassa-Holm and Degasperis-Procesi equations, *Am. J. Comput. Math.*, **5** (2015), 267–273. https://doi.org/10.4236/AJCM.2015.53024
2. A. Golbabai, M. Javidic, A spectral domain decomposition approach for the generalized Burgers-Fisher equation, *Chaos, Solitons Fractals*, **39** (2009), 385–392. https://doi.org/10.1016/j.chaos.2007.04.013
3. S. H. Hashemi, H. R. Mohammadi-Daniali, D. D. Ganji, Numerical simulation of the generalized Huxley equation by he's homotopy perturbation method, *Appl. Math. Comput.*, **192** (2007), 157–161. https://doi.org/10.1016/j.amc.2007.02.128
4. C. G. Zhu, R. H. Wang, Numerical solution of Burgers' equation by cubic B-spline quasi-interpolation, *Appl. Math. Comput.*, **208** (2009), 260–272. https://doi.org/10.1016/j.amc.2008.11.045

5. V. Gupta, M. K. Kadalbajoo, A singular perturbation approach to solve Burgers-Huxley equation via monotone finite difference scheme on layer-adaptive mesh, *Commun. Nonlinear Sci. Numer. Simul.*, **16** (2011), 1825–1844. https://doi.org/10.1016/j.cnsns.2010.07.020

6. M. Sari, G. Gürarslan, I. Dag, A compact finite difference method for the solution of the generalized Burgers-Fisher equation, *Numer. Methods Partial Differ. Equations*, **26** (2010), 125–134. https://doi.org/10.1002/num.20421

7. Y. Huang, F. Mohammadi-Zadeh, M. H. Noori-Skandari, H. Ahsani-Tehrani, E. Tohidi, Space-time Chebyshev spectral collocation method for nonlinear time-fractional Burgers equations based on efficient basis functions, *Math. Methods Appl. Sci.*, **44** (2021), 4117–4136. https://doi.org/10.1002/mma.7015

8. Y. Yang, J. D. Wang, S. Y. Zhang, E. Tohidi, Convergence analysis of space-time Jacobi spectral collocation method for solving time-fractional Schrödinger equations, *Appl. Math. Comput.*, **387** (2020), 124489. https://doi.org/10.1016/j.amc.2019.06.003

9. F. Mohammadizadeh, S. G. Georgiev, G. Rozza, E. Tohidi, S. Shateyi, Numerical solution of ψ-Hilfer fractional black-scholes via space-time spectral collocation method, *Alexandria Eng. J.*, **71** (2023), 131–145. https://doi.org/10.1016/j.aej.2023.03.007

10. Z. Chen, H. Zhang, H. Chen, ADI compact difference scheme for the two-dimensional integro-differential equation with two fractional Riemann-Liouville integral kernels, *Fractal Fract.*, **8** (2024), 707. https://doi.org/10.3390/fractalfract8120707

11. J. Lenells, Traveling wave solutions of the Camassa-Holm equation, *Int. J. Differ. Equations*, **217** (2005), 393–430. https://doi.org/10.1016/j.jde.2004.09.007

12. A. Parker, Y. Matsuno, The peakon limits of soliton solutions of the Camassa-Holm equation, *J. Phys. Soc. Jpn.*, **75** (2006), 124001. https://doi.org/10.1143/JPSJ.75.124001

13. G. P. Zhang, M. Zhang, New explicit exact traveling wave solutions of Camassa-Holm equation, *Appl. Anal.*, **104** (2021), 69–81. https://doi.org/10.1080/00036811.2021.1986024

14. H. Lundmark, Formation and dynamics of shock waves in the Degasperis-Procesi equation, *J. Nonlinear Sci.*, **17** (2007), 169–198. https://doi.org/10.1007/s00332-006-0803-3

15. A. Constantin, R. I. Ivannov, J. Lenells, Inverse svattering transform for the Degasperis-Procesi equation, *Nonlinearity*, **23** (2010), 2559–2575. https://doi.org/10.1088/0951-7715/23/10/012

16. B. F. Feng, K. Maruno, Y. Ohta, On the τ-functions of the Degaspeirs-Procesi equation, *J. Phys. A Math. Theor.*, **46** (2013), 045205. https://doi.org/10.1088/1751-8113/46/4/045205

17. M. Alquran, M. Ali, I. Jaradat, N. Al-Ali, Changes in the physical structures for new versions of the Degasperis-Procesi-Camassa-Holm model, *Chin. J. Phys.*, **71** (2021), 85–94. https://doi.org/10.1016/j.cjph.2020.11.010

18. A. H. Abdel-Kader, M. S. Abdel-Latif, New soliton solutions of the CH–DP equation using Lie symmetry method, *Mod. Phys. Lett. B*, **32** (2018), 1850234. https://doi.org/10.1142/S0217984918502342

19. S. Lafortune, D. E. Pelinovsky, Spectral instability of peakons in the b-family of the Camassa-Holm equations, *SIAM J. Math. Anal.*, **54** (2021), 4572–4590. https://doi.org/10.1137/21M1458776

20. X. B. Sun, J. B. Li, G. R. Chen, Bifurcations, exact peakon, periodic peakons and solitary wave solutions of generalized Camassa-Holm-Degasperis-Procosi type equation, *Int. J. Bifurcation Chaos*, **33** (2023), 2350124. https://doi.org/10.1142/S0218127423501249

21. M. Zhu, L. J. Guo, Y. Wang, Existence and uniqueness of the global conservative weak solutions to the cubic Camassa-Holm-Type equation, *Commun. Nonlinear Sci.*, **132** (2024), 107903. https://doi.org/10.1016/j.cnsns.2024.107903

22. K. Grunert, Uniqueness of dissipative solutions for the Camassa-Holm equation, *J. Differ. Equations*, **412** (2024), 474–528. https://doi.org/10.1016/j.jde.2024.08.036

23. Z. R. Liu, Z. Y. Ouyang, A note on solitary waves for modified forms of Camassa-Holm and Degasperis-Procesi equations, *Phys. Lett. A*, **366** (2007), 377–381. https://doi.org/10.1016/j.physleta.2007.01.074

24. R. Behera, M. Mehra, Approximate solution of modified Camassa-Holm and Degasperis-Procesi equations using wavelet optimized finite difference method, *Int. J. Wavelets Multiresolution Inf. Process.*, **11** (2013), 1350019. https://doi.org/10.1142/S0219691313500197

25. A. Kaur, V. Kanwar, H. Ramos, A coupled scheme based on uniform algebraic trigonometric tension B-spline and a hybrid block method for Camassa-Holm and Degasperis-Procesi equations, *Comput. Appl. Math.*, **43** (2024), 16. https://doi.org/10.1007/s40314-023-02530-4

26. C. R. Qi, L. P. Xue, Q. F. Zhang, Error estimate of an invariant-preserving fourth-order scheme for the Degasperis-Procesi equation with smooth solutions, *Appl. Math. Lett.*, **171** (2025), 109638. https://doi.org/10.1016/j.aml.2025.109638

27. M. S. Floater, K. Hormann, Barycentric rational interpolation with no poles and high rates of approximation, *Numer. Math.*, **107** (2007), 315–331. https://doi.org/10.1007/s00211-007-0093-y

28. J. P. Berrut, G. Klein, Recent advances in linear barycentric rational interpolation, *J. Comput. Appl. Math.*, **259** (2014), 95–107. https://doi.org/10.1016/j.cam.2013.03.044

29. A. P. Austin, K. Xu, On the numerical stability of the second barycentric formula for trigonometric interpolation in shifted equispaced points, *IMA J. Numer. Anal.*, **37** (2017), 1355–1374. https://doi.org/10.1093/imanum/drw038

30. A. Gillette, A. Rand, C. Bajaj, Error estimates for generalized barycentric interpolation, *Adv. Comput. Math.*, **37** (2012), 417–439. https://doi.org/10.1007/s10444-011-9218-z

31. S. Torkaman, M. Heydari, G. B. Loghmani, Piecewise barycentric interpolating functions for the numerical solution of Volterra integro-differential equations, *Math. Methods Appl. Sci.*, **45** (2022), 6030–6061. https://doi.org/10.1002/mma.8154

32. H. Y. Liu, J. Huang, Y. B. Pan, J. P. Zhang, Barycentric interpolation collocation method for solving linear and nonlinear high-dimensional Fredholm integral equations, *J. Comput. Appl. Math.*, **327** (2018), 141–154. https://doi.org/10.1016/j.cam.2017.06.004

33. J. Li, Y. L. Cheng, Linear barycentric rational collocation method for solving heat conduction equation, *Numer. Methods Partial Differ. Equations*, **37** (2021), 533–545. https://doi.org/10.1002/num.22539

34. J. Li, Linear barycentric rational collocation method for solving biharmonic equation, *Demonstr. Math.*, **55** (2022), 587–603. https://doi.org/10.1515/dema-2022-0151

35. J. Li, Barycentric rational collocation method for fractional reaction-diffusion equation, *AIMS Math.*, **8** (2023), 9009–9026. https://doi.org/10.3934/math.2023451

36. J. Li, Y. L. Cheng, Barycentric rational interpolation method for solving 3 dimensional convection-diffusion equation, *J. Approximation Theory*, **304** (2024), 106106. https://doi.org/10.1016/j.jat.2024.106106

37. S. P. Li, Z. Q. Wang, *Meshless Barycentric Interpolation Collocation Method-Algorithmics, Programs & Applications in Engineering*, Science Press, 2012.

38. Z. Q. Wang, S. P. Li, *Barycentric Interpolation Collocation Method for Nonlinear Problems*, National Defense Industry Press, 2015.

39. A. M. Wazwaz, Solitary wave solutions for modified forms of Degasperis-Procesi and Camassa-Holm equations, *Phys. Lett. A*, **352** (2006), 500–504. https://doi.org/10.1016/j.physleta.2005.12.036

40. P. Veeresha, D. G. Prakasha, Novel approach for modified forms of Camassa-Holm and Degasperis-Procesi equations using fractional operator, *Commun. Theor. Phys.*, **72** (2020), 105002. https://doi.org/10.1088/1572-9494/aba24b

41. J. P. Berrut, M. S. Floater, G. Klein, Convergence rates of derivatives of a family of barycentric rational interpolants, *Appl. Numer. Math.*, **61** (2011), 989–1000. https://doi.org/10.1016/j.apnum.2011.05.001

42. X. Shen, X. H. Yang, H. X. Zhang, The high-order ADI difference method and extrapolation method for solving the two-dimensional nonlinear parabolic evolution equations, *Mathematics*, **12** (2024), 3469. https://doi.org/10.3390/math12223469

AIMS Press